IJMMM International Journal of Minerals, Metallurgy and Materials 矿物冶金与材料学报（英文版）

Efficiency enhancement of $Cs_{0.1}(CH_3NH_3)_{0.9}PbI_3$ perovskite solar cell by surface passivation using iso-butyl ammonium iodide

Wakul Bumrungsan, Kritsada Hongsith, Vasan Yarangsi, Pisith Kumnorkeaw, Sukrit Sucharitakul, Surachet Phaduangdhitidhada, and Supab Choopun

Cite this article as:
Wakul Bumrungsan, Kritsada Hongsith, Vasan Yarangsi, Pisith Kumnorkeaw, Sukrit Sucharitakul, Surachet Phaduangdhitidhada, and Supab Choopun, Efficiency enhancement of $Cs_{0.1}(CH_3NH_3)_{0.9}PbI_3$ perovskite solar cell by surface passivation using iso-butyl ammonium iodide, *Int. J. Miner. Metall. Mater.*, 29(2022), No. 11, pp. 1963-1970. https://doi.org/10.1007/s12613-021-2382-3

View the article online at SpringerLink or IJMMM Webpage.

International Journal of Minerals, Metallurgy and Materials
Volume 29, Number 11, November 2022, Page 1963
https://doi.org/10.1007/s12613-021-2382-3

Efficiency enhancement of $Cs_{0.1}(CH_3NH_3)_{0.9}PbI_3$ perovskite solar cell by surface passivation using iso-butyl ammonium iodide

Wakul Bumrungsan[1,2], *Kritsada Hongsith*[1,2], *Vasan Yarangsi*[1,2], *Pisith Kumnorkeaw*[3], *Sukrit Sucharitakul*[1,2], *Surachet Phaduangdhitidhada*[1,2], *and Supab Choopun*[1,2]✉

1) Research Center in Physics and Astronomy, Department of Physics and Materials Science Faculty of Science, Chiang Mai University, Chiang Mai 50200, Thailand
2) Thailand Center Excellence in Physics, Ministry of Higher Education, Science, Research and Innovation, Bangkok 10400, Thailand
3) National Nanotechnology Center, National Science and Technology Development Agency, Pathum Thani 12120, Thailand
(Received: 30 April 2021; revised: 16 November 2021; accepted: 17 November 2021)

Abstract: Efficiency enhancement of $Cs_{0.1}(CH_3NH_3)_{0.9}PbI_3$ solar cell devices was performed by using iso-butyl ammonium iodide (IBA) passivated on $Cs_{0.1}(CH_3NH_3)_{0.9}PbI_3$ films. The n–i–p structure of perovskite solar cell devices was fabricated with the structure of FTO/SnO_2/$Cs_{0.1}(CH_3NH_3)_{0.9}PbI_3$ (FTO, i.e., fluorine doped tin oxide) and IBA/Spiro-OMeTAD/Ag. The effect of different weights of IBA passivated on Cs-doped perovskite solar cells (PSCs) was systematically investigated and compared with non-passivated devices. It was found that the 5-mg IBA-passivated devices exhibited a high power conversion efficiency (PCE) of 15.49% higher than 12.64% of non-IBA-passivated devices. The improvement of photovoltaic parameters of the 5-mg IBA-passivated device can be clearly observed compared to the Cs-doped device. The better performance of the IBA-passivated device can be confirmed by the reduction of PbI_2 phase in the crystal structure, lower charge recombination rate, lower charge transfer resistance, and improved contact angle of perovskite films. Therefore, IBA passivation on $Cs_{0.1}(CH_3NH)_{0.9}PbI_3$ is a promising technique to improve the efficiency of Cs-doped perovskite solar cells.

Keywords: perovskite solar cell; power conversion efficiency; surface passivation; cesium methylammonium lead iodide; iso-butyl ammonium iodide

1. Introduction

Perovskite solar cells (PSCs) have been much attention in a decade due to their excellent power conversion efficiency (PCE) compared to commercial Si solar cell devices [1–2]. The PCE of PSCs has dramatically increased in a few years since the first discovery by Miyasaka and co-workers [3]. Nowadays, the highest PCE of PSCs is 25.5% which is higher than the dye-sensitized solar cell (DSSC) and organic solar cell (OPV) [4]. Despite the great effort on PSCs efficiency improvement, the drawbacks of perovskite material and their organic material in PSCs such as poor stability make it cannot forward to commercialization based optoelectronic devices [5–6]. Also, several findings have indicated that perovskite films possess high bulk defects and trap states between perovskite and charge-transporting layers. These defects conduct faster recombination rates, a decrease of the open-circuit voltage which can be detrimental to the PCE and stability of PSCs [7–9]. To avoid these drawbacks of PSCs, several techniques have been used to improve both PCE and stability of PSCs such as encapsulation methods [10–11], using metal oxides for both electron transporting layer (ETL) and hole transporting layer (HTL) [12–14], self-assembly monolayers [15], surface passivation [16–18], etc. Among these methods, surface passivation is one of the techniques that can effectively improve charge transfer performance and reduce defect states in perovskite films.

Recently, large ammonium salt (aliphatic or alkylammonium salt), such as butyl-ammonium iodide (BAI) [19–20], phenyl ethyl ammonium iodide (PEAI) [21–22], and iso-butyl ammonium iodide (IBA) [23], has been much attention as candidates for surface passivation. The hydrophobic properties of the alkyl-group can enhance the hydrophobic surface of perovskite, influencing better humidity stability of PSCs [24–25]. Instantly, Zhu *et al*. [26] have demonstrated that 4-tert butyl benzyl ammonium iodide (tBBAi) passivated on 3D perovskite shows a PCE of 23.5% higher than 20% of the non-passivated device. The high PCE of the tBBAi-passivated devices can be elucidated by non-radiative recombination reduction. The tBBAi-passivated devices also reduce hysteresis and provide better humidity stability by hydrophobic umbrella protection of the tert-butyl group. Cho *et al*. [27] have indicated that IBA passivated on complex 3D perovskite enhances the PCE from 18% to 21.7%. The higher PCE can be contributed by lower non-radiative recombination and uniform perovskite crystalline. The humidity stability testing has also shown that the IBA-passivated device can excellently maintain 90% of the initial

✉ Corresponding author: Supab Choopun E-mail: supab99@gmail.com

PCE, better than that of the reference device. The better humidity can be supported by the hydrophobic properties of the bulky organic cation. From the above examples, the surface passivation approach can be considered as an effective method to improve both the PCE and stability of PSCs.

In this study, the effect of IBA passivated on the $Cs_{0.1}(CH_3NH_3)_{0.9}PbI_3$ perovskite for surface passivation approach is investigated. The highest PCE of 15.4% can be obtained by the 5-mg IBA-passivated device. The enhanced PCE from 12.64% to 15.49% can be discussed in terms of perovskite structure, charge recombination, charge transfer, and electron lifetime.

2. Experimental

2.1. Solar cell fabrication

Fluorine-doped tin oxide (FTO) coated glasses were ultrasonically cleaned with detergent, deionized water, acetone, and isopropanol, respectively, and dried with a nitrogen stream. Then, the FTO-coated glasses were cleaned by an ultraviolet (UV)–ozone system for 15 min before use. After that, tin oxide (SnO_2) was deposited onto FTO-coated glasses by spin coating. 22.5 mg of $SnCl_2{\cdot}2H_2O$ (99.8%, Sigma Aldrich) was dissolved in 1-mL ethanol. The $SnCl_2{\cdot}2H_2O$ solution was spun onto FTO substrates at 3000 r/min for 30 s and heated at 100°C for 10 min and at 180°C for 60 min with a similar technique as the previous report [28]. For perovskite preparation, 1 mmol lead iodide (PbI_2, 99.999%, Sigma Aldrich), 0.9 mmol methylammonium iodide (MAI, Greatcell Solar), and 0.1 mmol cesium iodide (CsI, Sigma Aldrich) were all dissolved in a mixed polar solvent (N,N-dimethylformamide (DMF) and dimethyl sulfoxide (DMSO) in the volume ratio of 4:1). The perovskite precursor solution was stirred and heated at 60°C overnight. To deposit perovskite films, the precursor solution was spun at two-step by 1000 r/min for 10 s and 4500 r/min for 30 s and heated at 100°C for 1 h. In this process, isopropanol (IPA) as an antisolvent was dropped on the perovskite precursor after 15 s at the second stage of spin coating. For the IBA passivated layer, different weights of IBA (3 mg, 5 mg, 10 mg, and 15 mg) were prepared by dissolving in IPA 1 mL for each condition. IBA precursor was dropped on perovskite surface by spin coating at 4000 r/min for 30 s and heated at 100°C for 15 min. For hole transporting layer deposition, 72.3-mg Spiro-OMeTAD was dissolved in 1-mL chlorobenzene doping with 39 μL of 4-tert-butyl pyridine and 20 μL of lithium-salt (520 mg of Li-bis(flurosulfonyl)imide in 1-mL acetonitrile). The hole transporting material was spun at 4000 r/min for 30 s. For metal electrodes, silver metal (Ag) was thermally deposited on the hole transporting layer by thermal evaporation under low pressure at 5×10^{-5} Pa. All process of the perovskite solar cell fabrication was carried out in a homemade glove box with a humidity controlling less than 10%.

2.2. Characterization

The X-ray diffraction patterns were performed by X-ray diffraction measurement (Rigaku miniflex II diffractometer with Cu K_α with a wavelength of 0.15406 nm). The steady-state photoluminescence spectroscopy was performed by a nitrogen laser with a wavelength of 337.1 nm. The PSC devices were characterized by current density–voltage (*J–V*) measurement. The *J–V* measurements were conducted by a *J–V* tester with the Ossila system (Automated-S211 (T2003B) with built-in software) under simulated solar light A.M.1.5. The current–voltage (*I–V*) curves of perovskite solar cell devices were symmetrically investigated at a scan rate of 1 ms per point from the voltage range of −0.2 to 1.2 V. The active area of incident solar light on the solar cells was defined by a photomask with an area of 0.04 cm^2. The charge dynamics of perovskite solar cells were measured via open-circuit voltage decay (OCVD) measurement. The electrochemical impedance spectroscopy (EIS) was measured by HIOKI 3522-50 LCR Hi tester.

3. Results and discussion

To investigate the effect of different IBA concentrations (3 mg, 5 mg, 10 mg, and 15 mg) on the photovoltaic properties of Cs-doped perovskite solar cell devices. The conventional perovskite solar cells architecture (n–i–p) of FTO/SnO_2/$Cs_{0.1}(CH_3NH_3)_{0.9}PbI_3$/IBA passivated layer/Spiro-OMeTAD/Ag are fabricated and illustrated as seen in the inset in Fig. 1(a). The photovoltaic parameters of solar cell devices are summarized in Table 1. As a result of the *J–V* characteristics in Fig. 1(a), The highest power conversion efficiency (PCE) of solar cell devices can be obtained from 5-mg IBA-passivated devices (blue line), reaching the highest PCE of 15.49% with short-circuit current density (J_{sc}), open-circuit voltage (V_{oc}), and fill factor (FF) of 22.20 mA/cm^2, 0.990 V, and 0.70, respectively. Meanwhile, the PCE of the Cs-doped (i.e., non-passivated) device shows only 12.64% which is lower than that of the 5-mg IBA-passivated device. In the case of 3 mg, it is found that the 3-mg IBA-passivated device exhibits lower PCE than the 5-mg IBA-passivated device and higher than the Cs-doped device. However, the 10-mg and 15-mg IBA-passivated devices show lower PCE compared to the Cs-doped device. Also, it can be observed that the V_{oc} of solar cell devices can be obviously enhanced by IBA surface passivation. The main reason for the efficiency enhancement of the 5-mg IBA-passivated device is an increase in J_{sc}, V_{oc}, and FF. Besides, the improved FF of the 5-mg IBA-passivated device can enhance the shunt resistance and provide low series resistance compared to other devices as seen in Table 1. Consequently, the 5-mg IBA-passivated device can enhance the efficiency of the Cs-doped perovskite solar cell device. The statistical distribution of PCE of Cs-doped PSCs passivated with different weights of IBA with the device number of $n = 10$ for each condition is shown in Fig. 1(b). The current density output at maximum power point of the solar cell devices as seen in Fig. 1(c) indicates that the decrease rate of current density at maximum power point of the 5-mg IBA-passivated device is slower than that of Cs-doped device. The incident-photon to current efficiency (IPCE) measurement of the Cs-doped device and the 5-mg IBA-passivated device is shown in Fig. 1(d). The IPCE value of the 5-

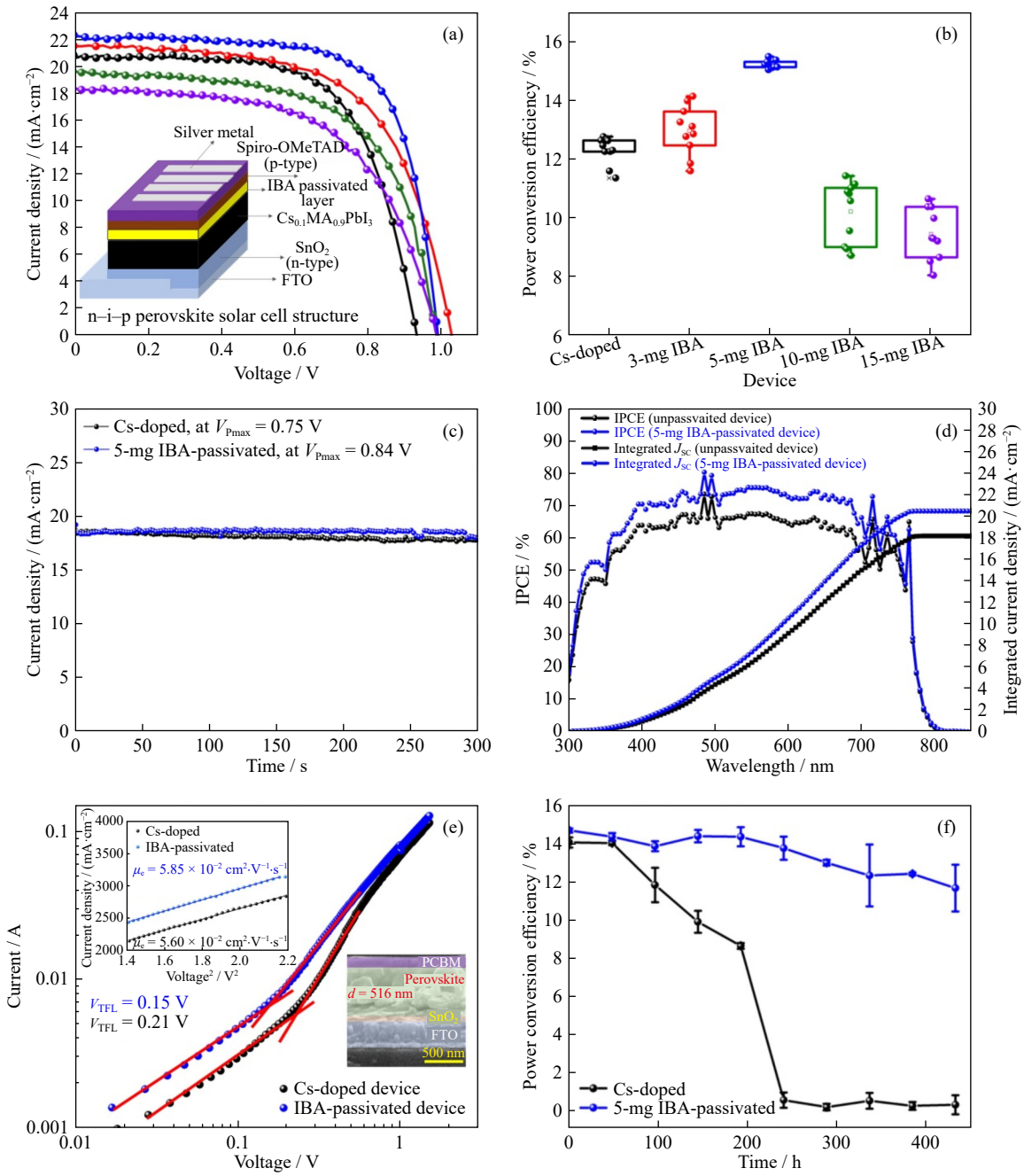

Fig. 1. (a) Current density versus voltage (*J–V*) characteristics of $Cs_{0.1}(CH_3NH_3)_{0.9}PbI_3$-based solar cell devices with different weights of IBA: Cs-doped (black line), 3 mg (red line), 5 mg (blue line), 10 mg (green line), and 15 mg (violet line). Inset is the schematic diagram of n–i–p convention structure of Cs-doped PSCs (FTO/SnO_2/$Cs_{0.1}MA_{0.9}PbI_3$/IBA passivated layer/Spiro-OMeTAD/Ag. (b) Statistical distribution of the PCE of Cs-doped PSCs passivated with different weights of IBA with the device number of n = 10 for each condition. (c) Current density output at maximum power point as a function of time under air ambient within 5 min. (d) IPCE and integrated current density of the $Cs_{0.1}(CH_3NH_3)_{0.9}PbI_3$-based solar cell devices with different weights of IBA. (e) *I–V* characteristics from the space charge limited current (SCLC) model of the electron only device (bias voltage from 0 to 1.5 V). Inset in the upper left conner is the linear relation of J and V^2; inset in the lower right conner is the perovskite device structure of FTO/SnO_2/perovskite/PCBM/Ag. (f) Stability of Cs-doped device and 5-mg IBA-passivated device without encapsulation at a relative humidity of 35%.

mg IBA-passivated device is higher than that of the Cs-doped device. The integrated current density of the Cs-doped device and the 5-mg IBA-passivated device is 18.17 and 20.49 mA/cm^2, respectively. The IPCE value of the 5-mg IBA-passivated device is higher than that of the Cs-doped device, confirming the current density of the solar cell device can be improved by 5-mg IBA passivation.

The trap state of perovskite layer is investigated by space-charge limit current (SCLC) of the electron-only device as seen in Fig. 1(e). The trap-filled limit voltage (V_{TFL}) of 5-mg IBA-passivated device (0.15 V) is lower than that of Cs-doped device (0.21 V), indicating the lower trap state of perovskite layer in the 5-mg IBA-passivated device. In addition, we have investigated the electron mobility of the solar cell

Table 1. Summary of photovoltaic parameters for Cs-doped perovskite solar cell devices passivated by different weights of IBA (3 mg, 5 mg, 10 mg, and 15 mg of IBA in IPA solution)

Device	Type	PCE / %	FF / %	J_{sc} / (mA·cm^{-2})	V_{oc} / V	R_{sh} / Ω	R_s / Ω
Cs-doped	Best	12.64	65.50	20.69	0.932	1234	7.09
	(Average)	(12.24 ± 0.57)	(64.77 ± 0.97)	(20.26 ± 0.81)	(0.932 ± 0.008)		
3-mg IBA-passivated	Best	13.62	61.52	21.54	1.028	1075	8.19
	(Average)	(12.74 ± 0.79)	(61.52 ± 1.88)	(20.39 ± 1.53)	(1.017 ± 0.006)		
5-mg IBA-passivated	Best	15.49	70.47	22.20	0.990	1333	4.38
	(Average)	(15.23 ± 0.13)	(70.15 ± 0.25)	(21.95 ± 0.24)	(0.989 ± 0.004)		
10-mg IBA-passivated	Best	11.92	61.35	19.59	0.993	902	9.43
	(Average)	(11.54 ± 0.29)	(61.27 ± 1.82)	(19.08 ± 0.83)	(0.987 ± 0.012)		
15-mg IBA-passivated	Best	10.65	58.27	19.54	0.985	606	17.23
	(Average)	(9.36 ± 1.18)	(56.06 ± 2.97)	(17.20 ± 1.80)	(0.974 ± 0.017)		

devices performed by the linear relation of J–V^2 as seen in the inset in Fig. 1(e). The electron mobility (μ_e) can be extracted by the following Mott-gurney law: $J = 9\varepsilon\varepsilon_0\mu V^2/(8d^3)$, where ε and ε_0 are dielectric constant of perovskite and permittivity of free space, and d is the thickness of perovskite film [29]. From the J–V^2 plot, it can be obtained that the μ_e of Cs-doped device and 5-mg IBA passivated device are 5.60×10^{-2} and 5.85×10^{-2} cm^2·V^{-1}·s^{-1}, respectively, indicating the improvement of the electron mobility by 5-mg IBA passivation on Cs-doped perovskite solar cell.

The stability of the Cs-doped and 5-mg IBA-passivated devices is also compared as seen in Fig. 1(f). The 5-mg IBA-passivated device exhibits good stability compared to the Cs-doped device after 400 h at air ambient with a relative humidity of 35%.

The hysteresis effect of solar cell devices is also investigated as shown in Fig. 2(a) and (b). The hysteresis index (HI) in Eq. (1) is applied to elucidate the hysteresis effect of solar cell devices,

$$\mathrm{HI} = \frac{\mathrm{PCE}_{\mathrm{reverse}} - \mathrm{PCE}_{\mathrm{forward}}}{\mathrm{PCE}_{\mathrm{reverse}}} \quad (1)$$

where $\mathrm{PCE}_{\mathrm{forward}}$ and $\mathrm{PCE}_{\mathrm{reverse}}$ represent power conversion efficiency measured by forward biased voltage and power conversion efficiency measured by reverse biased voltage, respectively.

The hysteresis index of Cs-doped perovskite and 5-mg IBA-passivated solar cell device are 0.291 and 0.158, respectively. The decrease of hysteresis index in the case of 5-mg IBA-passivated device indicates that small change of J–V characteristic of solar cell device which is better than that of Cs-doped perovskite device. The small change of J–V characteristic of solar cell devices can be referred to better ionic and electronic response in solar cell devices [30]. Consequently, the 5-mg IBA-passivated device provides a better ionic and electronic response than the non-passivated device. To further investigate the effect of IBA passivated on Cs-doped perovskite, the 5-mg IBA-passivated and the Cs-doped devices will be compared and discussed.

The surface morphology properties of Cs-doped perovskite passivated with different weights of IBA are characterized by scanning electron microscopy (SEM) as seen in Fig 3. The SEM image of Cs-doped film is shown in Fig. 3(a). The surface morphology of Cs-doped perovskite after IBA passivating with 3 mg and 5 mg of IBA indicates that small amounts of 2D perovskite are covered on Cs-doped perovskite as seen in Fig. 3(b) and (c). The small amount of 2D perovskite on Cs-doped perovskite can improve the perovskite surface as confirmed by increasing of current in the solar cell devices. However, the surface of Cs-doped perovskite is fully covered by 2D and quasi 2D perovskite in the case of 10-mg and 15-mg IBA-passivated films as seen in Fig. 3(d) and (e). The fully covered 2D and quasi 2D perovskite on 3D perovskite with random orientation can suppress charge transportation, referring to the decrease of current in solar cell devices [31–32].

The structural properties of Cs-doped perovskite films passivated by different IBA concentrations are characterized using the X-ray diffraction (XRD) pattern as seen in Fig. 4.

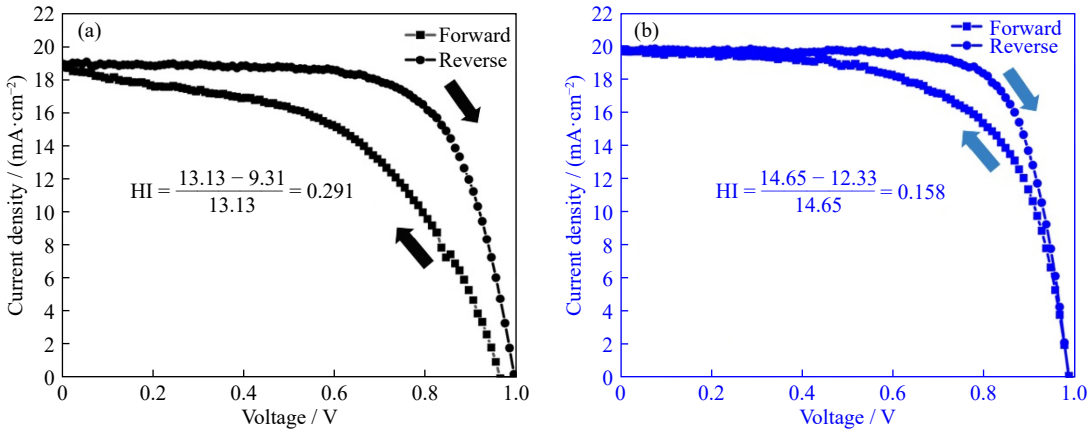

Fig. 2. Hysteresis of (a) Cs-doped PSCs and (b) 5-mg IBA-passivated PSCs.

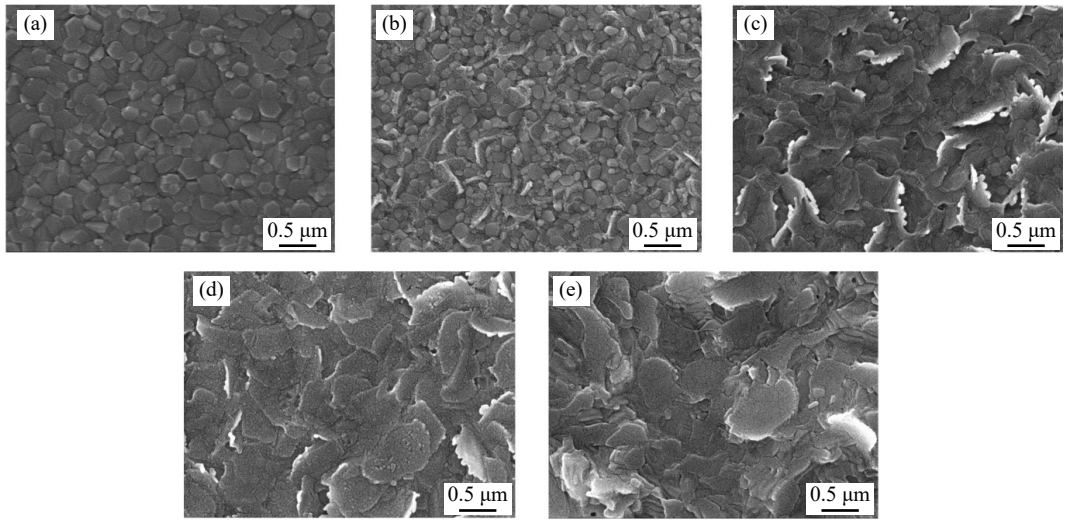

Fig. 3. SEM images of Cs-doped perovskite surfaces passivated with different weights of IBA with magnification of 30000: (a) without passivation, (b) 3 mg IBA, (c) 5 mg IBA, (d) 10 mg IBA, and (e) 15 mg IBA.

The peaks of Cs-doped film exhibits 2θ of 14.2°, 20.1°, 28.4°, 31.9°, 40.6°, and 43.1°, corresponding to the (110), (112), (220), (310), (224), and (314), respectively [33]. The small peaks of PbI_2 phase at 12.7° are also observed in the perovskite patterns in the Cs-doped, 3-mg IBA-passivated, and 5-mg IBA-passivated films; it is well-known that the exceeding PbI_2 phase in perovskite films can suppress light absorption and reduce the performance of PSC devices. In order to investigate the exceeding PbI_2 phase in the perovskite films, the intensity ratio of PbI_2 at 12.7° and the perovskite peak at 14.2° defined as $R = I_{12.7}/(I_{12.7} + I_{14.2})$ are performed to quantify the PbI_2 phase in perovskite films [34]. It is found that the R of the 5-mg IBA-passivated film (0.07) shows lower than that of Cs-doped film (0.21), indicating the 5-mg IBA passivated on Cs-doped perovskite film can reduce the PbI_2 phase which supports better perovskite structure properties. In the case of 5-mg IBA-passivated film, the 2D phase of $(IBA)_2PbI_4$ can be observed at the peak of 6.7°, suggesting 2D perovskite phase forms on Cs-doped perovskite film. With the increase of IBA weight of 10 mg and 15 mg on the Cs-doped perovskite films, other phases occur in the perovskite structure including 6.7° and 9.2°, which represent the

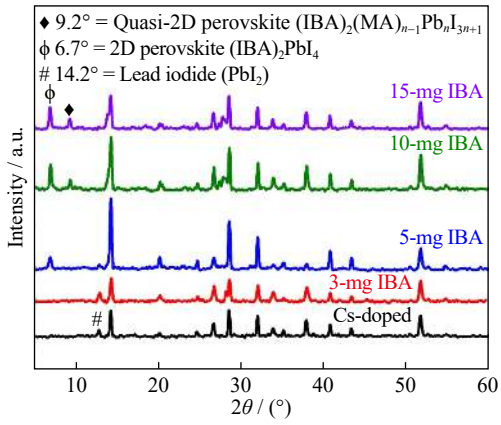

Fig. 4. X-ray diffraction patterns of Cs-doped perovskite films by passivating with different weights of IBA (0 mg, 3 mg, 5 mg, 10 mg, and 15 mg).

2D perovskite phase $(IBA)_2PbI_4$ and quasi 2D perovskite phase $(IBA)_n(MA)_{n-1}PbI_{3n+1}$, respectively [27], This suggests that the 2D perovskite and quasi 2D perovskite can be formed on the Cs-doped perovskite surface. Typically, the 2D and quasi 2D perovskite phase formation on perovskite with random plane direction suppress charge transfer of solar cell device [35], supporting the current-density reduction of the 5-mg and 10-mg IBA-passivated devices as seen in Fig. 1(b).

The absorbance spectra of perovskite films are illustrated in Fig. 5(a). It can be observed that there is no change in the absorbance of perovskite films. The absorbance in the range of 550–800 nm of both Cs-doped and 5-mg IBA-passivated films shows the same absorption edge of perovskite films and is about 764 nm, relating to the bandgap of 1.62 eV. It can be indicated that 5-mg IBA-passivated device cannot change the light absorption of Cs-doped perovskite films. Also, the optical properties of Cs-doped film and 5-mg IBA-passivated film are investigated by steady-state photoluminescence (PL) as seen in Fig. 5(b). The PL spectra of Cs-doped film exhibit PL peaks at the wavelength of 764 nm as same as the absorption edge in UV–visible spectra. In the case of the 5-mg IBA-passivated film, it can be found that the decrease of the 3D perovskite peak at 764 nm and the increase of the 2D perovskite peak at 523 nm can be seen. The increase of the 2D phase can be also confirmed the formation of the IBA-passivated layer top on perovskite film.

To investigate the effect of charge recombination, the open-circuit voltage decay is performed as shown in Fig. 6(a). The reduction of V_{oc} after tuning light off indicates the charge dynamic behavior of the solar cell devices as a function of time. The biexponential decay relation in Eq. (2) can be applied to elucidate these phenomena. The biexponential fitting curves are plotted as seen in Fig. 6(a).

$$V(t) = A_1 e^{-\frac{t}{T_1}} + A_2 e^{-\frac{t}{T_2}} \quad (2)$$

$$T_{ave} = A_1^* T_1 + A_2^* T_2 \quad (3)$$

where A_1 and A_2 are time dependence coefficients of amplitude fraction; A_1^* and A_2^* are normalized time dependence

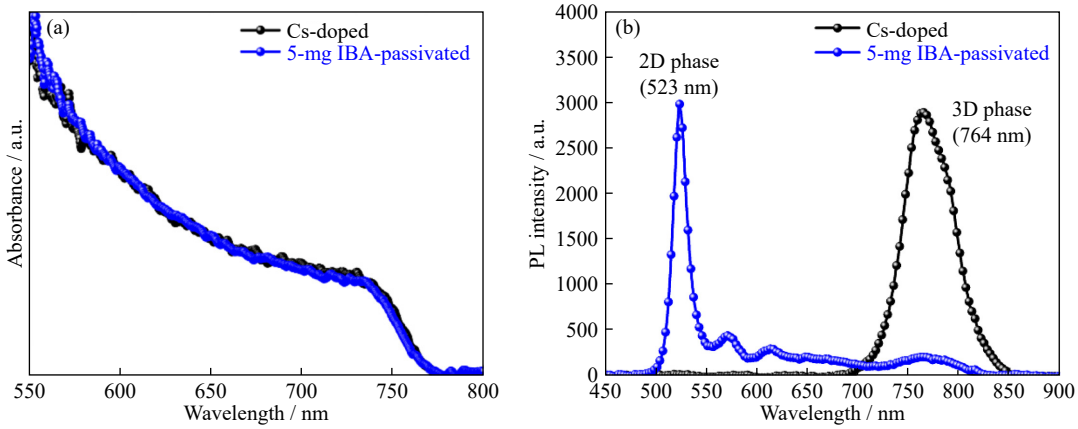

Fig. 5. Optical properties comparison between Cs-doped perovskite and 5-mg IBA-passivated perovskite film: (a) UV–visible spectra and (b) PL-spectra.

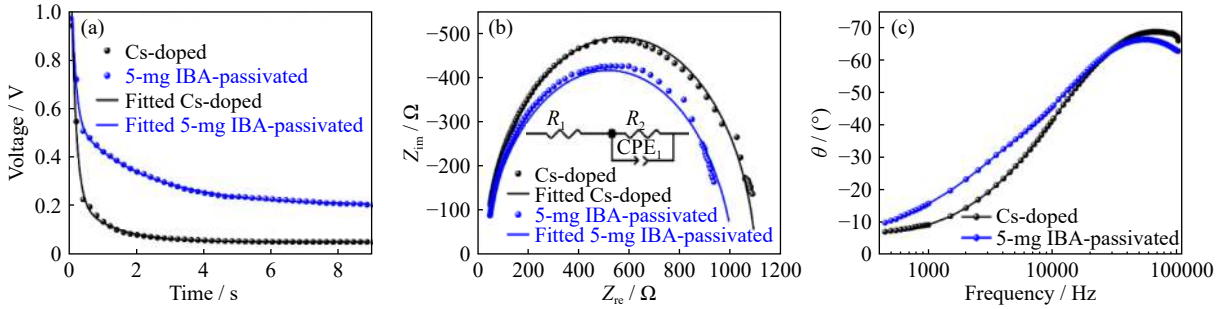

Fig. 6. (a) Open-circuit voltage decay (OCVD) of Cs-doped and 5-mg IBA-passivated PSCs fitting by the biexponential decay curve of voltage as a function of time by experiment data (dot) and fitted data (line). Electrochemical impedance spectroscopy performed in the range of frequency 100 kHz to 450 Hz. (b) Nyquist plot of Cs-doped device and 5-mg IBA-passivated devices. Inset is the equivalent circuit where R_1 and R_2 represent series resistance and charge transfer resistance, respectively. (c) Bode phase plot of Cs-doped and 5-mg IBA-passivated devices.

coefficients of amplitude fraction; T_1 and T_2, are fast and slow time decay components, respectively. The average time decay coefficient (T_{ave}) can be performed by Eq. (3). The T_{ave} can be used to elucidate the charge recombination rate of solar cell devices. The longer T_{ave} is defined to a longer charge recombination rate. In contrast, the smaller value of T_{ave} is defined to shorter charge recombination.

From the OCVD results, the time decay parameter can be summarized in Table 2. It can be seen that the average time decay coefficient of the 5-mg IBA-passivated device indicates a longer T_{ave} than that of the Cs-doped device, which can be indirectly interpreted as the reduction of charge recombination rate by the 5-mg IBA passivation on perovskite surface. The lower charge recombination rate indicates to lower trap defect of solar cell devices, confirming higher V_{oc} of the 5-mg IBA-passivated device [36].

To investigate the electrical properties of solar cell devices, The Nyquist plot and bode phase plot of Cs-doped and 5-mg IBA-passivated devices were carried out by EIS equivalent circuit applied in EIS spectra is illustrated in the inset of Fig. 6(b). From the equivalent circuit, the EIS spectra can be fitted to quantify series resistance (R_s) and charge transfer resistance (R_{ct}), which is summarized in Table 3. For fitting the EIS parameter, it can be found that the R_{ct} of Cs-doped and the 5-mg IBA-passivated devices are 1071 and 991 Ω, respectively. Consequently, the EIS parameter from the Nyquist plot indicates that the 5-mg IBA-passivated device exhibits a lower semicircle radius than the Cs-doped device, which can be indicated to lower charge transfer resistance, supporting to higher J_{sc} of the 5-mg IBA-passivated device.

To investigate the electron lifetime of solar cell devices, the bode phase plot can be also performed as seen in Fig. 6(c). The electron lifetime (τ) can be calculated by Eq. (4) [37–38].

$$\tau = \frac{1}{\omega_{max}} = \frac{1}{2\pi f_{max}} \tag{4}$$

where ω_{max} is maximum angular frequency and f_{max} is maximum frequency. The f_{max} can be obtained from the fre-

Table 2. Summary of biexponential parameters A_1^*, T_1, A_2^*, T_2, and T_{ave}

Device	A_1^*	T_1 / s	A_2^*	T_2 / s	T_{ave} / s
Cs-doped	0.86	0.14	0.14	1.1	0.267
5-mg IBA-passivated	0.72	0.12	0.28	2.1	0.670

Table 3. Summary of EIS parameter from Nyquist plot (R_s, R_{ct}, f_{max}, and τ)

Device	R_s / Ω	R_{ct} / Ω	f_{max} / Hz	τ / μs
Cs-doped	23.82	1071	68000	2.34
5-mg IBA-passivated	17.55	991	53000	3.00

quency at the highest bode phase peak. From the bode phase spectra, it can be found that the f_{max} of Cs-doped and 5-mg IBA-passivated devices are 68 and 53 kHz, respectively. Also, the electron lifetimes of the Cs-doped and the 5-mg IBA passivated devices can be calculated to be 2.34 and 3.00 μs, respectively, indicating longer electron lifetimes of solar cell devices can be improved by IBA passivation on perovskite surface.

In addition, the wettability of perovskite films is also observed by contact angle measurement as seen in Fig. 7(a) and (b). It is found that the contact angle of 5 mg IBA-passivated perovskite film (55.1°) is higher than that of the Cs-doped device (42.3°), suggesting the lower surface energy and higher hydrophobic of the 5-mg IBA-passivated perovskite film. The higher hydrophobic film by IBA-treated film can be indirectly interpreted as better stability from humidity.

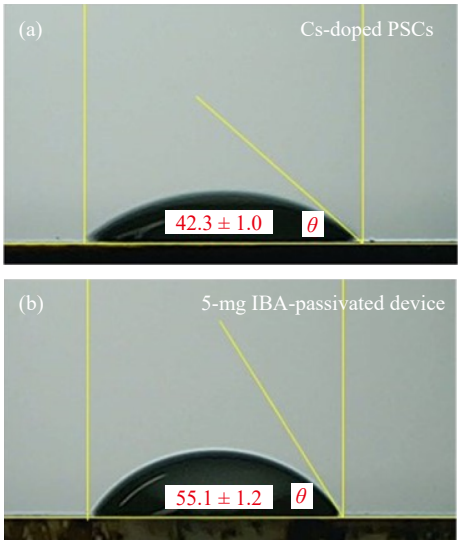

Fig. 7. Contact angle measurement of (a) Cs-doped and (b) 5-mg IBA-passivated solar cell devices. θ represents the wetting angle.

4. Conclusion

The efficiency of $Cs_{0.1}(CH_3NH_3)_{0.9}PbI_3$ perovskite solar cell is successfully enhanced by iso-butyl ammonium iodide surface passivation. The 5-mg IBA passivated on Cs-doped perovskite solar cell device shows a champion PCE of 15.49% which is higher than 12.64% of non-passivated Cs-doped devices. The enhanced PCE of solar cell devices can be elucidated in terms of the improvement of perovskite phase structure, better carrier charge transfer, and lower charge recombination rate in solar cell devices. SEM images reveal the surface medication of Cs-doped perovskite by IBA passivation. XRD analysis indicates that the PbI_2 phase at 14.2° in perovskite can be reduced after passivating by IBA and verifying the existence of 2D and quasi 2D phase on perovskite structure. UV–Vis spectra exhibit the same bandgap of 1.69 eV of 5-mg IBA-passivated film and Cs-doped perovskite film. The lower charge transfer resistance of the 5-mg IBA-passivated device indicates the better charge carrier transfer. The lower charge recombination rate of 5-mg IBA-passivated device implies lower trap defect of solar cell devices, confirming higher V_{oc} of the 5-mg IBA-passivated device. Also, the higher contact angle of the 5-mg IBA-passivated devices provides a higher hydrophobic perovskite surface compared to the Cs-doped device, suggesting better humidity stability. Moreover, the 5-mg IBA-passivated device exhibits good stability compared to the Cs-doped device after 400 h at air ambient with a relative humidity of 35%. Consequently, surface passivation by using IBA is an alternative candidate for the efficiency enhancement of Cs-doped perovskite solar cell devices.

Acknowledgements

This research work was partially supported by Chiang Mai University. Wakul Bumrungsan would like to acknowledge financial support from the Development and Promotion of Science and Technology Talent Project (DPST) and Graduate School, Chiang Mai University.

Conflict of Interest

Authors declare no potential conflict of interest.

References

[1] J.Y. Kim, J.W. Lee, H.S. Jung, H. Shin, and N.G. Park, High-efficiency perovskite solar cells, *Chem. Rev.*, 120(2020), No. 15, p. 7867.

[2] R. Wang, M. Mujahid, Y. Duan, Z.K. Wang, J.J. Xue, and Y. Yang, A review of perovskites solar cell stability, *Adv. Funct. Mater.*, 29(2019), No. 47, art. No. 1808843.

[3] A. Kojima, K. Teshima, Y. Shirai, and T. Miyasaka, Organometal halide perovskites as visible-light sensitizers for photovoltaic cells, *J. Am. Chem. Soc.*, 131(2009), No. 17, p. 6050.

[4] National Renewable Energy Laboratory, *Best Research-Cell Efficiency Chart* [2021-02]. http://www.nrel.gov/pv/cell-efficiency.html

[5] D. Wang, M. Wright, N.K. Elumalai, and A. Uddin, Stability of perovskite solar cells, *Sol. Energy Mater. Sol. Cells*, 147(2016), p. 255.

[6] G.D. Niu, X.D. Guo, and L.D. Wang, Review of recent progress in chemical stability of perovskite solar cells, *J. Mater. Chem. A*, 3(2015), No. 17, p. 8970.

[7] J. Peng, Y.L. Wu, W. Ye, D.A. Jacobs, H.P. Shen, X. Fu, Y.M. Wan, T. Duong, N.D. Wu, C. Barugkin, H.T. Nguyen, D.Y. Zhong, J.T. Li, T. Lu, Y. Liu, M.N. Lockrey, K.J. Weber, K.R. Catchpole, and T.P. White, Interface passivation using ultrathin polymer–fullerene films for high-efficiency perovskite solar cells with negligible hysteresis, *Energy Environ. Sci.*, 10(2017), No. 8, p. 1792.

[8] Z.P. Wang, Q.Q. Lin, F.P. Chmiel, N. Sakai, L.M. Herz, and H.J. Snaith, Efficient ambient-air-stable solar cells with 2D–3D heterostructured butylammonium-caesium-formamidinium lead halide perovskites, *Nat. Energy*, 2(2017), No. 9, art. No. 17135.

[9] K. Wojciechowski, T. Leijtens, S. Siprova, C. Schlueter, M.T. Hörantner, J.T.W. Wang, C.Z. Li, A.K.Y. Jen, T.L. Lee, and H.J. Snaith, C60 as an efficient n-type compact layer in perovskite solar cells, *J. Phys. Chem. Lett.*, 6(2015), No. 12, p. 2399.

[10] F. Matteocci, L. Cinà, E. Lamanna, S. Cacovich, G. Divitini, P.A. Midgley, C. Ducati, and A. Di Carlo, Encapsulation for long-term stability enhancement of perovskite solar cells, *Nano Energy*, 30(2016), p. 162.
[11] Z.Y. Fu, M. Xu, Y.S. Sheng, Z.B. Yan, J. Meng, C.H. Tong, D. Li, Z.N. Wan, Y. Ming, A.Y. Mei, Y. Hu, Y.G. Rong, and H.W. Han, Encapsulation of printable mesoscopic perovskite solar cells enables high temperature and long-term outdoor stability, *Adv. Funct. Mater.*, 29(2019), No. 16, art. No. 1809129.
[12] H. Zhang, H. Wang, W. Chen, and A.K.Y. Jen, $CuGaO_2$: A promising inorganic hole-transporting material for highly efficient and stable perovskite solar cells, *Adv. Mater.*, 29(2017), No. 8, art. No. 1604984.
[13] J. Tirado, M. Vásquez-Montoya, C. Roldán-Carmona, M. Ralaiarisoa, N. Koch, M.K. Nazeeruddin, and F. Jaramillo, Air-stable n–i–p planar perovskite solar cells using nickel oxide nanocrystals as sole hole-transporting material, *ACS Appl. Energy Mater.*, 2(2019), No. 7, p. 4890.
[14] J.B. You, L. Meng, T.B. Song, T.F. Guo, Y. Yang, W.H. Chang, Z.R. Hong, H.J. Chen, H.P. Zhou, Q. Chen, Y.S. Liu, N. De Marco, and Y. Yang, Improved air stability of perovskite solar cells via solution-processed metal oxide transport layers, *Nat. Nanotechnol.*, 11(2016), No. 1, p. 75.
[15] L. Chu and L.M. Ding, Self-assembled monolayers in perovskite solar cells, *J. Semicond.*, 42(2021), No. 9, art. No. 090202.
[16] Q. Jiang, Y. Zhao, X.W. Zhang, X.L. Yang, Y. Chen, Z.M. Chu, Q.F. Ye, X.X. Li, Z.G. Yin, and J.B. You, Surface passivation of perovskite film for efficient solar cells, *Nat. Photonics*, 13(2019), No. 7, p. 460.
[17] J.M. Xia, C. Liang, S.L. Mei, H. Gu, B.C. He, Z.P. Zhang, T.H. Liu, K.Y. Wang, S.S. Wang, S. Chen, Y.Q. Cai, and G.C. Xing, Deep surface passivation for efficient and hydrophobic perovskite solar cells, *J. Mater. Chem. A*, 9(2021), No. 5, p. 2919.
[18] L. Chu, Pseudohalide anion engineering for highly efficient and stable perovskite solar cells, *Matter*, 4(2021), No. 6, p. 1762.
[19] L. Yangi, Y.W. Li, Y.X. Pei, J.Q. Wang, H. Lin, and X. Li, A novel 2D perovskite as surface "patches" for efficient flexible perovskite solar cells, *J. Mater. Chem. A*, 8(2020), No. 16, p. 7808.
[20] Y.F. Wang, H. Xu, F. Wang, D.T. Liu, H. Chen, H.L. Zheng, L. Ji, P. Zhang, T. Zhang, Z.D. Chen, J. Wu, L. Chen, and S.B. Li, Unveiling the guest effect of N-butylammonium iodide towards efficient and stable 2D–3D perovskite solar cells through sequential deposition process, *Chem. Eng. J.*, 391(2020), art. No. 123589.
[21] J. Horn, M. Scholz, K. Oum, T. Lenzer, and D. Schlettwein, Influence of phenylethylammonium iodide as additive in the formamidinium tin iodide perovskite on interfacial characteristics and charge carrier dynamics, *APL Mater.*, 7(2019), No. 3, art. No. 031112.
[22] Y. Zhang, S. Jang, I.W. Hwang, Y.K. Jung, B.R. Lee, J.H. Kim, K.H. Kim, and S.H. Park, Bilateral interface engineering for efficient and stable perovskite solar cells using phenylethylammonium iodide, *ACS Appl. Mater. Interfaces*, 12(2020), No. 22, p. 24827.
[23] Y.H. Liu, S. Akin, A. Hinderhofer, F.T. Eickemeyer, H.W. Zhu, J.Y. Seo, J.H. Zhang, F. Schreiber, H. Zhang, S.M. Zakeeruddin, A. Hagfeldt, M.I. Dar, and M. Grätzel, Stabilization of highly efficient and stable phase-pure $FAPbI_3$ perovskite solar cells by molecularly tailored 2D-overlayers, *Angew. Chem. Int. Ed.*, 59(2020), No. 36, p. 15688.
[24] H.Y. Zheng, G.Z. Liu, L.Z. Zhu, J.J. Ye, X.H. Zhang, A. Alsaedi, T. Hayat, X. Pan, and S.Y. Dai, The effect of hydrophobicity of ammonium salts on stability of quasi-2D perovskite materials in moist condition, *Adv. Energy Mater.*, 8(2018), No. 21, art. No. 1800051.
[25] Y.T. Zheng, T.T. Niu, X.Q. Ran, J. Qiu, B.X. Li, Y.D. Xia, Y.H. Chen, and W. Huang, Unique characteristics of 2D Ruddlesden–Popper (2DRP) perovskite for future photovoltaic application, *J. Mater. Chem. A*, 7(2019), No. 23, p. 13860.
[26] H.W. Zhu, Y.H. Liu, F.T. Eickemeyer, L.F. Pan, D. Ren, M.A. Ruiz-Preciado, B. Carlsen, B.W. Yang, X.F. Dong, Z.W. Wang, H.L. Liu, S.R. Wang, S.M. Zakeeruddin, A. Hagfeldt, M.I. Dar, X.G. Li, and M. Grätzel, Tailored amphiphilic molecular mitigators for stable perovskite solar cells with 23.5% efficiency, *Adv. Mater.*, 32(2020), No. 12, art. No. 1907757.
[27] Y. Cho, A.M. Soufiani, J.S. Yun, J. Kim, D.S. Lee, J. Seidel, X.F. Deng, M.A. Green, S.J. Huang, and A.W.Y. Ho-Baillie, Mixed 3D–2D passivation treatment for mixed-cation lead mixed-halide perovskite solar cells for higher efficiency and better stability, *Adv. Energy Mater.*, 8(2018), No. 20, art. No. 1703392.
[28] V. Yarangsi, K. Hongsith, S. Sucharitakul, A. Ngamjarurojana, A. Tuantranont, P. Kumnorkaew, Y.X. Zhao, S. Phadungdhitidhada, and S. Choopun, Interface modification of SnO_2 layer using p–n junction double layer for efficiency enhancement of perovskite solar cell, *J. Phys. D: Appl. Phys.*, 53(2020), No. 50, art. No. 505103.
[29] K.C. Hsiao, M.H. Jao, B.T. Li, T.H. Lin, S.H.C. Liao, M.C. Wu, and W.F. Su, Enhancing efficiency and stability of hot casting p–i–n perovskite solar cell via dipolar ion passivation, *ACS Appl. Energy Mater.*, 2(2019), No. 7, p. 4821.
[30] S.N. Habisreutinger, N.K. Noel, and H.J. Snaith, Hysteresis index: A figure without merit for quantifying hysteresis in perovskite solar cells, *ACS Energy Lett.*, 3(2018), No. 10, p. 2472.
[31] Y.P. Li, H.J. Li, L.W. Tian, Q.Y. Wang, F.K. Wu, F. Zhang, L. Du, and Y.L. Huang, Vertical phase segregation suppression for efficient FA-based quasi-2D perovskite solar cells via HCl additive, *J. Mater. Sci.: Mater. Electron.*, 31(2020), No. 15, p. 12301.
[32] X.Q. Zhang, G. Wu, S.D. Yang, W.F. Fu, Z.Q. Zhang, C. Chen, W.Q. Liu, J.L. Yan, W.T. Yang, and H.Z. Chen, Vertically oriented 2D layered perovskite solar cells with enhanced efficiency and good stability, *Small*, 13(2017), No. 33, art. No. 1700611.
[33] H. Choi, J. Jeong, H.B. Kim, S. Kim, B. Walker, G.H. Kim, and J.Y. Kim, Cesium-doped methylammonium lead iodide perovskite light absorber for hybrid solar cells, *Nano Energy*, 7(2014), p. 80.
[34] M. Adnan and J.K. Lee, Highly efficient planar heterojunction perovskite solar cells with sequentially dip-coated deposited perovskite layers from a non-halide aqueous lead precursor, *RSC Adv.*, 10(2020), No. 9, p. 5454.
[35] F. Huang, P. Siffalovic, B. Li, S.X. Yang, L.X. Zhang, P. Nadazdy, G.Z. Cao, and J.J. Tian, Controlled crystallinity and morphologies of 2D Ruddlesden-Popper perovskite films grown without anti-solvent for solar cells, *Chem. Eng. J.*, 394(2020), art. No. 124959.
[36] I. Hwang, M. Baek, and K. Yong, Core/shell structured TiO_2/CdS electrode to enhance the light stability of perovskite solar cells, *ACS Appl. Mater. Interfaces*, 7(2015), No. 50, p. 27863.
[37] G.T. Dai, L. Zhao, J. Li, L. Wan, F. Hu, Z.X. Xu, B.H. Dong, H.B. Lu, S.M. Wang, and J.G. Yu, A novel photoanode architecture of dye-sensitized solar cells based on TiO_2 hollow sphere/nanorod array double-layer film, *J. Colloid Interface Sci.*, 365(2012), No. 1, p. 46.
[38] J.T. Park, D.K. Roh, W.S. Chi, R. Patel, and J.H. Kim, Fabrication of double layer photoelectrodes using hierarchical TiO_2 nanospheres for dye-sensitized solar cells, *J. Ind. Eng. Chem.*, 18(2012), No. 1, p. 449.